Received 11 September 2019; revised 13 October 2019 and 5 November 2019; accepted 6 November 2019. Date of publication 11 September 2019; date of current version 18 November 2019. The review of this article was arranged by Editor S. Reggiani.

Digital Object Identifier 10.1109/JEDS.2019.2952314

High Performance and Highly Robust AlN/GaN HEMTs for Millimeter-Wave Operation

KATHIA HARROUCHE, RIAD KABOUCHE, ETIENNE OKADA, AND FARID MEDJDOUB

CNRS-IEMN, Institut d'Electronique, de Microélectronique et de Nanotechnologie, 59652 Villeneuve-d'Ascq, France

CORRESPONDING AUTHOR: K. HARROUCHE (e-mail: kathia.harrouche.etu@univ-lille.fr)

This work was supported in part by the French RENATECH Network, in part by the French Government through Program PIA EQUIPEX LEAF under Grant ANR-11-EQPX-0025, and in part by the French Defense Procurement Agency (DGA) under Project EDA-EuGaNiC and Contract FUI-VeGaN.

ABSTRACT We report on a 3 nm AlN/GaN HEMT technology for millimeter-wave applications. Electrical characteristics for a 110 nm gate length show a maximum drain current density of 1.2 A/mm, an excellent electron confinement with a low leakage current below 10 μA/mm, a high breakdown voltage and a F_T/F_{max} of 63/300 GHz at a drain voltage of 20V. Despite residual trapping effects, state of the art large signal characteristics at 40 GHz and 94 GHz are achieved. For instance, an outstanding power added efficiency of 65% has been reached at $V_{DS} = 10$V in pulsed mode at 40 GHz. Also, an output power density of 8.3 W/mm at $V_{DS} = 40$V is obtained associated to a power added efficiency of 50%. At 94 GHz, a record CW output power density for Ga-polar GaN transistors has been reached with 4 W/mm. Additionally, room temperature preliminary robustness assessment at 40 GHz has been performed at $V_{DS} = 20$V. 24 hours RF monitoring showed no degradation during and after the test.

INDEX TERMS GaN, HEMTs, output power density (P_{out}), power added efficiency (PAE), Q-band, reliability, W-band.

I. INTRODUCTION

Gallium Nitride (GaN)-based RF power devices have made substantial progress in the last decade, which will enable new applications such as military wireless communication, SATCOM and 5G next generation of mobile broadband. Indeed, those applications operating at high frequency need compact systems, for which the power-added-efficiency (PAE) is a critical parameter. That is why, achieving both high PAE and output power density (P_{OUT}) in the millimeter-wave (mmW) range represents currently one of the key goal for the GaN technology. High Electron Mobility Transistors (HEMT) on SiC have already demonstrated attractive efficiencies up to Ka-Band [1]–[5] but limited data have been reported so far in the Q-Band [6]–[8] and above [9]–[15]. To obtain very high frequency performance, it is necessary to shrink the device dimensions and wisely optimize the epilayer stack, especially the barrier thickness. Thus, the gate length scaling must be linked to the reduction of the gate to channel distance in order to avoid short channel effects [16]. We have previously demonstrated the interest of the AlN/GaN heterostructure for mmW applications including the use of an ultrathin 4.0 nm barrier combined with an optimized Carbon-doped buffer [17]. Downscaling the barrier thickness could not only improve the power gain and thus the power-added-efficiency but also reduce the strain enabling a better device reliability. In this work, we report on a further scaled 3.0 nm barrier AlN/GaN HEMTs power performance up to the W-Band. Besides the state-of-the-art performance, a preliminary large signal robustness assessment at 40 GHz on these mmW devices is demonstrated.

II. DEVICE FABRICATION

The heterostructure has been grown by metal organic chemical vapor deposition (MOCVD) on 4-in. SiC substrates. Fig. 1 shows the cross section of the HEMT structure consisting in an AlN nucleation layer, a carbon-doped GaN buffer layer followed by an undoped 100 nm GaN channel and a 3.0 nm ultrathin AlN barrier layer. The HEMT was capped with a 10 nm thick in-situ SiN layer used both as

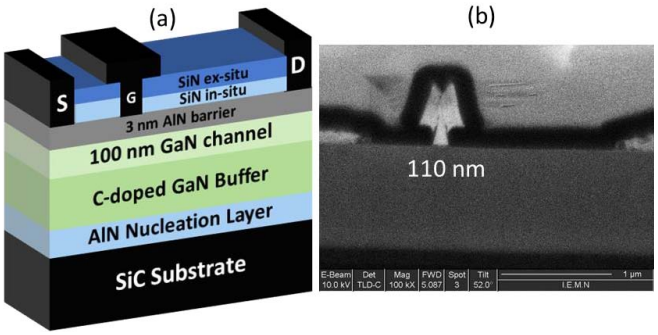

FIGURE 1. **Schematic cross section of the fabricated (a) 2×25 μm AlN/GaN-on-SiC HEMTs and (b) FIB view of a 110 nm T-gate.**

early passivation as well as to reduce the surface trapping effects. Room-temperature Hall effect measurements showed a high electron sheet concentration of 1.9×10^{13} cm^{-2} with an electron mobility of 965 cm^2/Vs. A Ti/Al/Ni/Au metal stack annealed at 850°C for 1 min has been used to form the source-drain ohmic contacts directly on top of the AlN barrier by etching the in-situ Si_3N_4 layer. Then, Ni/Au T-gates with various lengths were defined by e-beam lithography. The SiN underneath the gate was fully removed by SF_6 plasma etching through the e-beam lithography. Finally, a 200 nm PECVD Si_3N_4 layer was deposited as final passivation.

III. DC AND SMALL SIGNAL CHARACTERISTICS

DC measurements have been carried out with a Keysight A2902A static modular and source monitor. Fig. 2 shows the output and transfer characteristics of the fabricated 2×25 μm AlN/GaN-on-SiC HEMTs. The gate-source voltage was swept from −4 V to +2 V with a step of 1 V. The maximum drain current density I_{Dmax} is about 1.2 A/mm for GD = 0.5 μm (shown in Fig. 2(a)). An identical pinch-off voltage $V_{TH} = -2$ V (shown in Fig. 2(b)) is observed for the different gate lengths with a drain leakage current below 20 μA/mm, which reflects the absence of short channel effects and the excellent electron confinement. A transconductance of 400 mS/mm has been measured. However, this value can be significantly increased by reducing the access resistances, as the contact resistances are as high as 0.45 Ω.mm as extracted by transmission line measurements.

The Fig. 3(a) shows the strong impact of the gate-to-drain distance on the 3-terminal breakdown voltage as excepted. The breakdown voltage of the 110 nm technology scales well as a function of GD with 50V for GD = 0.5 μm to more than 130V for GD = 2.5 μm. A pronounced Kink effect can be noticed within the output characteristics, which confirms the rather strong trapping effects [18], [19] as seen from the gate and drain lag due to the residual surface and buffer traps. This is confirmed in Fig. 3(b) showing the open channel DC pulsed measurements at $V_{GS} = +2$ V for various quiescent bias points corresponding to the gate length (L_G) of 110 nm and gate-drain distance (GD) of 0.5 μm. The charge trapping

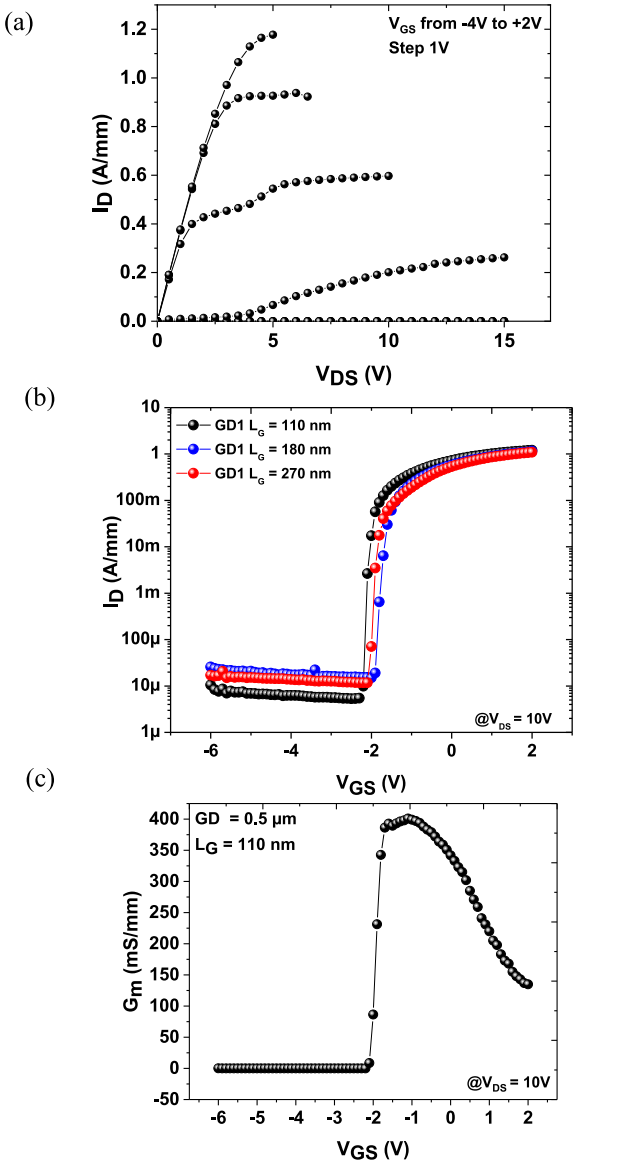

FIGURE 2. **(a) Output, (b) transfer characteristics and (c) transconductance of AlN/GaN HEMT 2x25 μm devices.**

is mainly attributed to the proximity of the carbon-doping with the 2DEG, which is known to generate trapping [20]. Also, the gate lag reveals the presence of traps in the vicinity of the gate most probably generated during the local SiN etching prior to the gate metal deposition.

The S-parameters have been measured from 250 MHz to 67 GHz with a Rhode and Schwarz ZVA67GHz network analyzer (see Fig. 4). As expected, the current gain extrinsic cut-off frequency (F_T) slightly decreases with V_{DS} and L_G (shown in Fig. 4(a)). It can be pointed out that there is a large room for F_T improvement by both reducing the contact resistances and the gate length. The maximum oscillation frequency (F_{max}) increases as a function of V_{DS}, which in turn confirms the absence of short channel effects. F_T/F_{max} of 63/300 GHz are achieved at $V_{DS} = 20$V for a GD = 0.5 μm

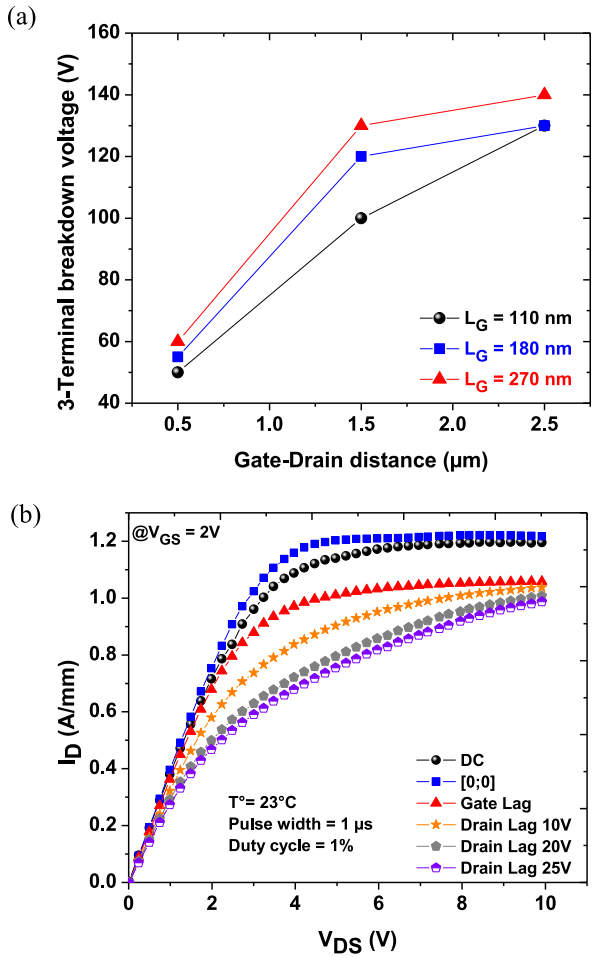

FIGURE 3. 3-Terminal breakdown voltage (a) and Pulsed I_D-V_{DS} characteristics with three different quiescent bias points: Cold point: V_{DS0} = 0V, V_{GS0} = 0V, gate lag: V_{DS0} = 0V, V_{GS0} = −6V and drain lag: V_{DS0} = [10V, 20V, 25V], V_{GS0} = −6V (b) of AlN/GaN HEMT 2x25 µm devices.

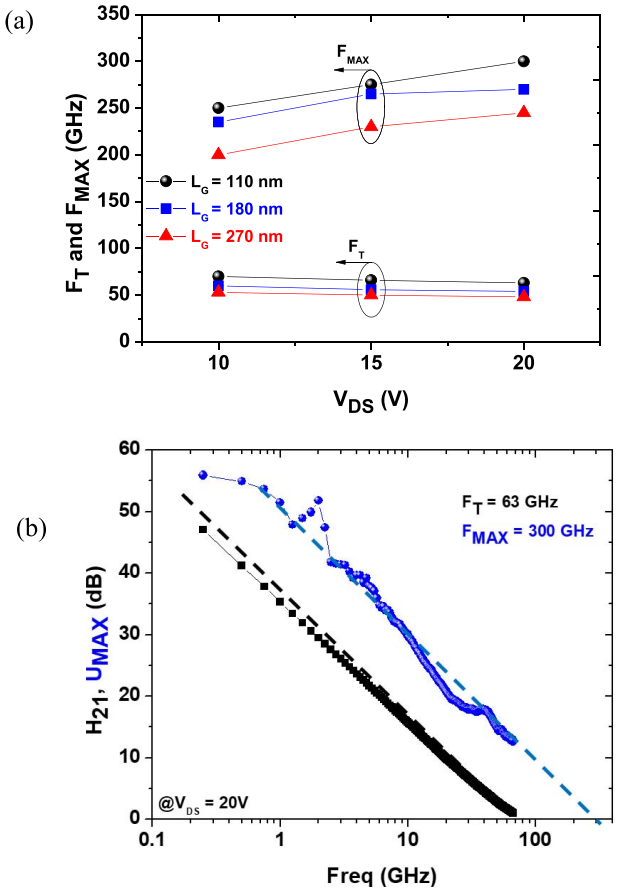

FIGURE 4. F_T, F_{max} as a function of V_{DS} for various gate lengths (a) and F_T/F_{max} at V_{DS} = 20V with L_G = 110 nm (b).

and L_G = 110 nm (Fig. 4(b)). For instance, the power gain is in excess of 17 dB at 40 GHz for the shortest design. The F_{max}/F_T ratio close to 5 is attributed to the highly favorable aspect ratio: gate length/gate-to-channel distance (>25).

IV. 40 GHZ LARGE SIGNAL CHARACTERISTICS:

Large signal characterizations have been carried out at 40 GHz on a nonlinear vector network analyzer system (Keysight Network Analyser: PNA-X, N5245A-NVNA) capable of on-wafer large signal device characterization up to the Q-band in continuous and pulsed mode. Further details of this specific power bench can be found in [21]. Fig. 6 shows typical pulsed (cold point, 1 µs width and 1% duty cycle) power performances at V_{DS} = 10V and 20V of a 2×50 µm transistor with L_G = 110 nm and GD = 0.5 µm. A saturated P_{OUT} of 1.6 W/mm associated to an outstanding PAE above 65% (corresponding to a drain efficiency of 75%) at V_{DS} = 10V and around 60% with a saturated P_{OUT} of 3.8 W/mm at V_{DS} = 20V (Z_L = 0.8 <45°>). Nevertheless, despite

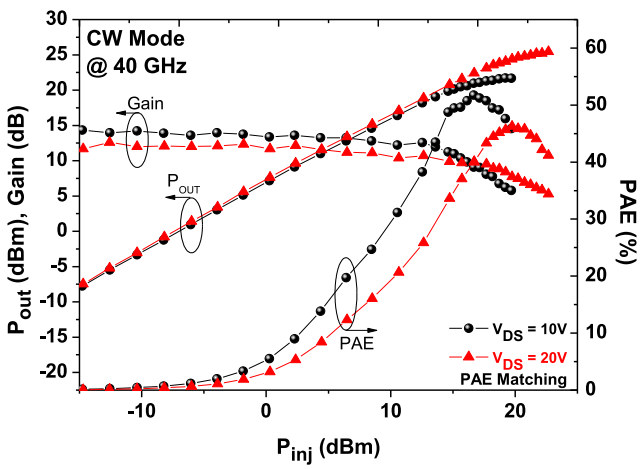

FIGURE 5. CW power performances of an AlN/GaN HEMT 2x50 µm with L_G = 110 nm for GD = 0.5 µm at V_{DS} = 10V, 20V.

the strong trapping effects, a high PAE around 50% up to V_{DS} = 20V is obtained in CW as shown Fig. 5. In order to reach higher drain voltage (i.e., high power density), larger GD have been also measured.

Fig. 8 shows the pulsed power performances for GD = 1.5 µm and various V_{DS} up to 40V. In this case, the PAE

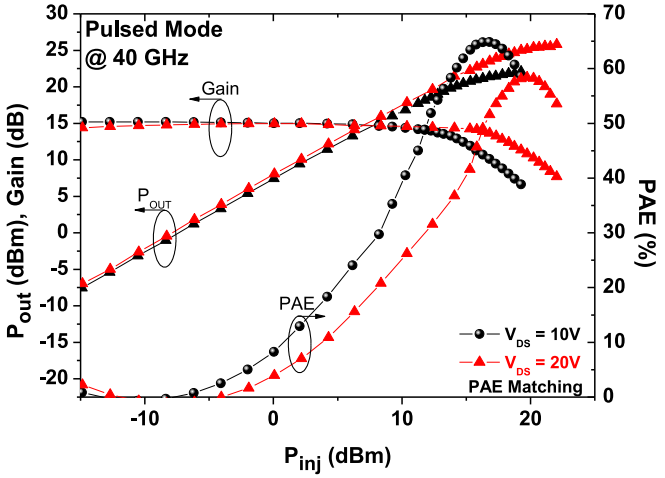

FIGURE 6. Pulsed power performances of an AlN/GaN HEMT 2x50 μm with L_G = 110 nm for GD = 0.5 μm at V_{DS} = 10V, 20V.

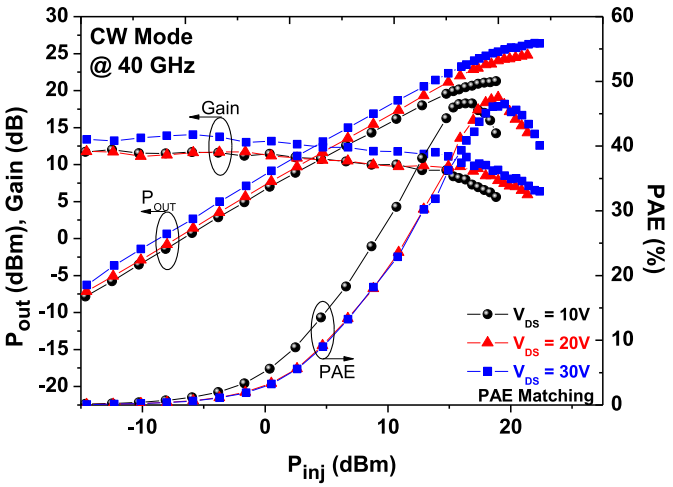

FIGURE 7. CW power performances of a 2x50 μm AlN/GaN HEMT (L_G = 110 nm, GD = 1.5μm) at V_{DS} = 10V, 20V and 30V.

remains around 60% up to V_{DS} = 30V (Z_L = 0.9 <35°>) with a saturated P_{OUT} of 5.4 W/mm (PAE matching). Due to the limitation of the test bench, only power matching was achievable at V_{DS} = 40V. At this drain voltage, the PAE is maintained above 50% with a saturated P_{OUT} as high as 8.3 W/mm. The comparison between large signal CW and pulsed mode is presented in Fig. 9. The gap in term of performances between CW and pulsed mode reflects the trapping effects observed in the DC pulsed characteristics and thus a large room for improvement for the CW performances.

V. 94 GHZ LARGE SIGNAL CHARACTERISTICS

CW large signal characterizations at 94 GHz have then been performed on the same devices. A state-of-the-art P_{OUT} = 4 W/mm in CW mode is observed with a PAE of 14.3% at V_{DS} = 20V as shown in Fig. 10. It appears that with a gate length of 110 nm, high performances in W-band can be achieved with this technology.

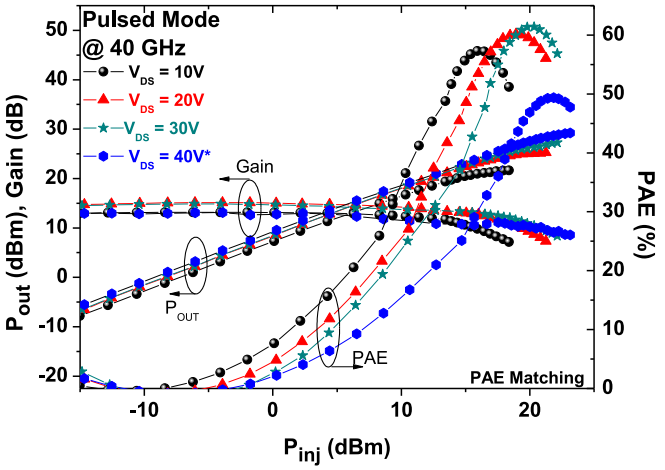

FIGURE 8. Pulsed power performances of a 2x50 μm AlN/GaN HEMT (L_G = 110 nm, GD = 1.5μm) at V_{DS} = 10V, 20V, 30V and 40V*. ***Power matching only.***

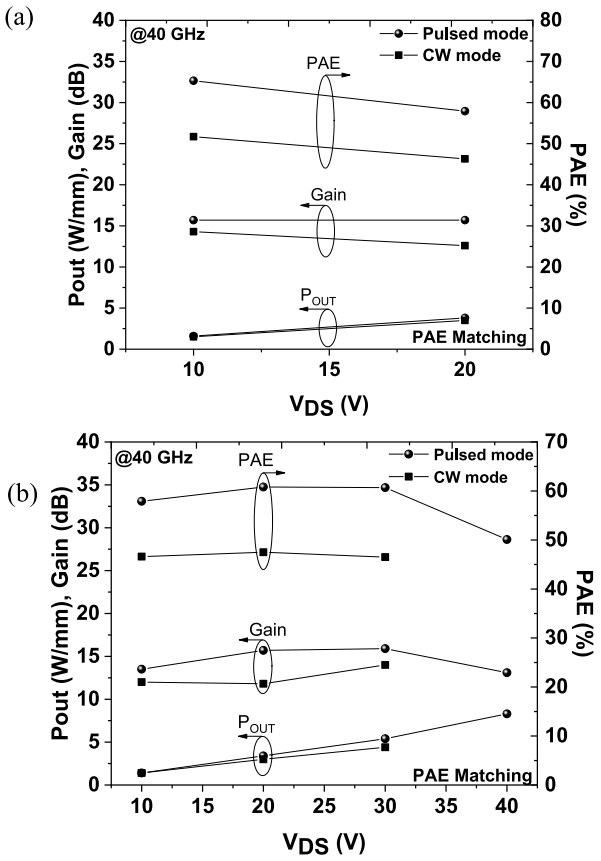

FIGURE 9. CW (circle) and pulsed (square) P_{OUT}, PAE and gain as a function of V_{DS} at 40 GHz of HEMT 2x50 μm for GD = 0.5μm (a) and GD = 1.5μm (b).

Downscaling the gate length together with reduced contact resistances will certainly allow even higher performance, especially an improved PAE. Fig. 11(a) shows that these devices are favorably comparable to the Ga-Polar HEMTs state-of-the-art both in Q-band [1]–[8] and W-band as shown in Fig. 11(b) [9]–[15].

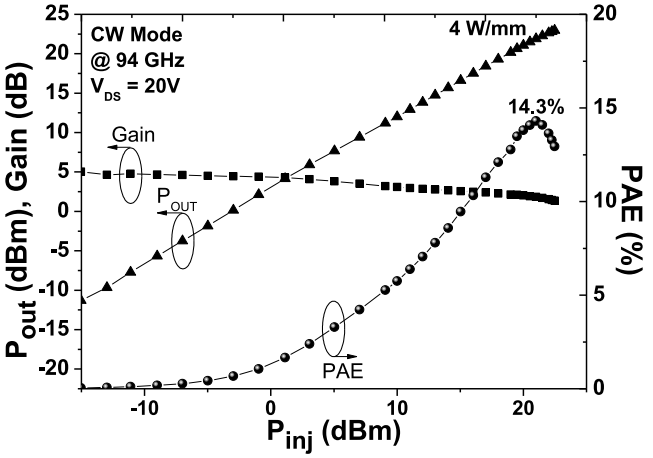

FIGURE 10. CW power performances of an AlN/GaN HEMT 2x25 μm with L_G = 110 nm for GD = 0.5μm at V_{DS} = 20V.

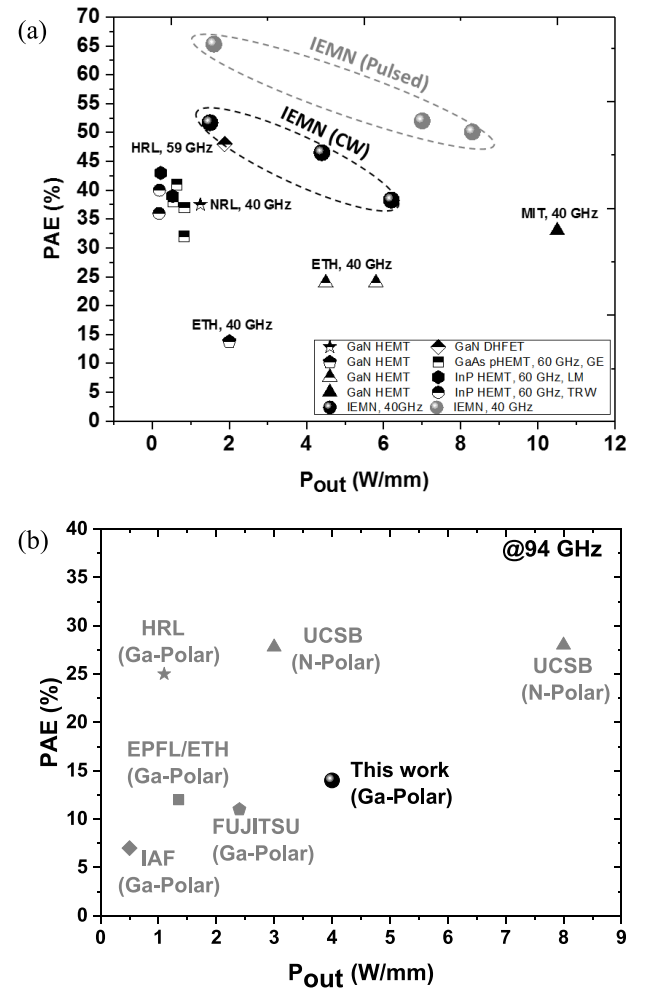

FIGURE 11. Benchmark of GaN HEMT devices in Ka-Q-Band (a) and W-Band (b).

VI. SHORT TERM LARGE SIGNAL ROBUSTNESS ASSESSMENT

With the aim of assessing the robustness of these devices, the P_{OUT}, PAE, Gain and the gate leakage current during the CW large signal measurements at 40 GHz have been monitored during 24 hours (by step of 8 hours) at room temperature (shown in Fig. 12 and 13). The injected power has been fixed to 18.5 dBm on a 2×50 μm transistor (GD = 1.5 μm and L_G = 110 nm) at the peak PAE (around 50 %) with V_{DS} = 20V. These measurements reveal that up to 24 hours, no-degradation is observed both in terms of performances and leakage current. It is interesting to note that the rather strong trapping effects do not favor any device degradation as seen in several previous reports [22]–[24]. The device robustness is attributed to the optimized T-gate and the surface passivation process.

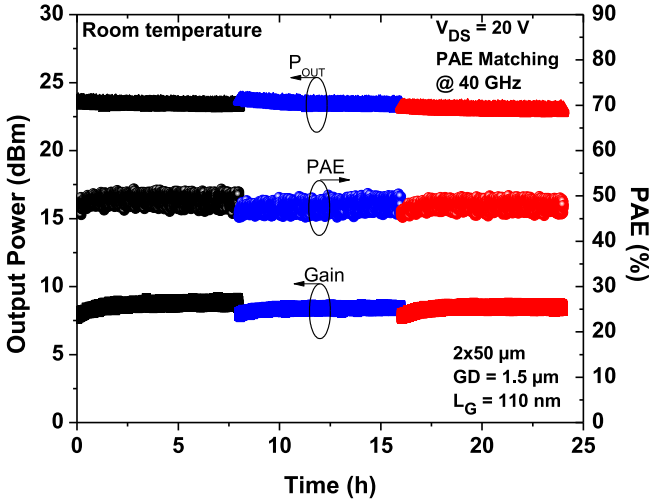

FIGURE 12. CW P_{OUT}, PAE and gain at 40 GHz at V_{DS} = 20V during 24 hours.

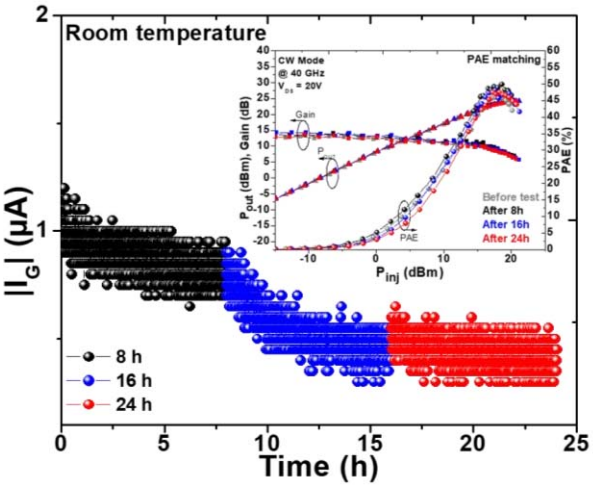

FIGURE 13. Gate current at V_{DS} = 20V during 24 hours.

VII. CONCLUSION

We have developed high frequency AlN/GaN HEMTs grown on SiC substrate. This technology enables to deliver high power density together with state-of-the-art PAE in pulsed mode (> 65%) and CW (> 50%) at 40 GHz. Moreover,

high pulsed $P_{OUT} > 8$ W/mm with a PAE of 50% at $V_{DS} = 40$V has been achieved. CW performance at 94 GHz of the same devices shows an outstanding P_{OUT} of 4 W/mm at $V_{DS} = 20$ V. This achievement is attributed to the optimization of both material, design and processing quality enabling a high electron confinement together with reduced short channel effects under high electric field. In addition, preliminary large signal robustness assessment at 40 GHz shows no degradation of the devices under a monitoring during 24 hours owing to the in-situ SiN superior surface passivation enhancing the surface robustness. This is believed to be the first GaN HEMT report of high performances up to 94 GHz demonstrated simultaneously with stability during 24-h stress-test at 40 GHz.

ACKNOWLEDGMENT

The authors would like to acknowledge the company EpiGaN for high material quality delivery.

REFERENCES

[1] B. Romanczyk *et al.*, "Demonstration of constant 8 W/mm power density at 10, 30, and 94 GHz in state-of-the-art millimeter-wave N-polar GaN MISHEMTs," *IEEE Trans. Electron Devices*, vol. 65, no. 1, pp. 45–50, Jan. 2018, doi: 10.1109/TED.2017.2770087.

[2] J. S. Moon *et al.*, "55% PAE and high power Ka-band GaN HEMTs with linearized transconductance via $n+$ GaN source contact ledge," *IEEE Electron Device Lett.*, vol. 29, no. 8, pp. 834–837, Aug. 2008, doi: 10.1109/LED.2008.2000792.

[3] A. Crespo *et al.*, "High-power Ka-band performance of AlInN/GaN HEMT with 9.8-nm-thin barrier," *IEEE Electron Device Lett.*, vol. 31, no. 1, pp. 2–4, Jan. 2010, doi: 10.1109/LED.2009.2034875.

[4] J. S. Moon *et al.*, "Gate-recessed AlGaN-GaN HEMTs for high-performance millimeter-wave applications," *IEEE Electron Device Lett.*, vol. 26, no. 6, pp. 348–350, Jun. 2005, doi: 10.1109/LED.2005.848107.

[5] T. Palacios *et al.*, "High-power AlGaN/GaN HEMTs for Ka-band applications," *IEEE Electron Device Lett.*, vol. 26, no. 11, pp. 781–783, Nov. 2005, doi: 10.1109/LED.2005.857701.

[6] E. Dogmus, R. Kabouche, A. Linge, E. Okada, M. Zegaoui, and F. Medjdoub, "High power, high PAE Q−band sub−10 nm barrier thickness AlN/GaN HEMTs," *Physica Status Solidi a*, vol. 214, no. 8, pp. 1–4, 2017, doi: 10.1002/pssa.201600797.

[7] B. P. Downey, D. J. Meyer, D. S. Katzer, J. A. Roussos, M. Pan, and X. Gao, "SiN_x /InAlN/AlN/GaN MIS-HEMTs with 10.8 $THz \cdots$ V Johnson figure of merit," *IEEE Electron Device Lett.*, vol. 35, no. 5, pp. 527–529, May 2014, doi: 10.1109/LED.2014.2313023.

[8] D. Marti, S. Tirelli, A. R. Alt, J. Roberts, and C. R. Bolognesi, "150-GHz cutoff frequencies and 2-W/mm output power at 40 GHz in a millimeter-wave AlGaN/GaN HEMT technology on silicon," *IEEE Electron Device Lett.*, vol. 33, no. 10, pp. 1372–1374, Oct. 2012, doi: 10.1109/LED.2012.2204855.

[9] B. Romanczyk *et al.*, "W-band N-polar GaN MISHEMTs with high power and record 27.8% efficiency at 94 GHz," in *Proc. Int. Electron Device Meeting*, San Francisco, CA, USA, 2016, pp. 67–70, doi: 10.1109/IEDM.2016.7838339.

[10] D. Marti *et al.*, "94-GHz large-signal operation of AlInN/GaN high-electron-mobility transistors on silicon with regrown ohmic contacts," *IEEE Electron Device Lett.*, vol. 36, no. 1, pp. 17–19, Jan. 2015, doi: 10.1109/LED.2014.2367093.

[11] Y. Niida *et al.*, "3.6 W/mm high power density W-band InAlGaN/GaN HEMT MMIC power amplifier," in *Proc. IEEE Topical Conf. Power Amplifiers Wireless Radio Appl. (PAWR)*, Austin, TX, USA, 2016, pp. 24–26, doi: 10.1109/PAWR.2016.7440153.

[12] A. Margomenos *et al.*, "GaN technology for E, W and G-band applications," in *Tech. Dig. IEEE Compd. Semicond. Integr. Circuit Symp. (CSIC)*, 2014, pp. 1–4, doi: 10.1109/CSICS.2014.6978559.

[13] F. Medjdoub, M. Zegaoui, and N. Rolland, "Beyond 100 GHz AlN/GaN HEMTs on silicon substrate," *Electron. Lett.*, vol. 47, no. 24, pp. 1345–1346, Nov. 2011, doi: 10.1049/el.2011.3166.

[14] K. Makiyama *et al.*, "Collapse-free high power InAlGaN/GaN-HEMT with 3 W/mm at 96 GHz," in *Tech. Dig. Int. Electron Devices Meeting (IEDM)*, vol. 2016. Washington, DC, USA, 2015, pp. 9.1.1–9.1.4, doi: 10.1109/IEDM.2015.7409659.

[15] K. Shinohara *et al.*, "220GHz f_T and 400GHz f_{max} in 40-nm GaN DH-HEMTs with re-grown ohmic," in *Tech. Dig. Int. Electron Devices Meeting (IEDM)*, 2010, pp. 30.1.1–30.1.4, doi: 10.1109/IEDM.2010.5703448.

[16] G. H. Jessen *et al.*, "Short-channel effect limitations on high-frequency operation of AlGaN/GaN HEMTs for T-gate devices," *IEEE Trans. Electron Devices*, vol. 54, no. 10, pp. 2589–2597, Oct. 2007, doi: 10.1109/TED.2007.904476.

[17] R. Pecheux, R. Kabouche, E. Okada, M. Zegaoui, and F. Medjdoub, "C-doped AlN/GaN HEMTs for high efficiency mmW applications," in *Proc. Int. Workshop Integr. Nonlin. Microw. Millimetre Wave Circuits (INMMIC)*, 2018, doi: 10.1109/INMMIC.2018.8430021.

[18] M. Wang and K. J. Chen, "Kink effect in AlGaN/GaN HEMTs induced by Drain and gate pumping," *IEEE Electron Device Lett.*, vol. 32, no. 4, pp. 482–484, Apr. 2011, doi: 10.1109/LED.2011.2105460.

[19] G. Meneghesso, F. Zanon, M. J. Uren, and E. Zanoni, "Anomalous kink effect in GaN high electron mobility transistors," *IEEE Electron Device Lett.*, vol. 30, no. 2, pp. 100–102, Feb. 2009, doi: 10.1109/LED.2008.2010067.

[20] I. Chatterjee *et al.*, "Impact of buffer charge on the reliability of carbon doped AlGaN/GaN-on-Si HEMTs," in *Proc. IEEE Int. Rel. Phys. Symp. (IRPS)*, Pasadena, CA, USA, 2016, pp. 4A.4.1–4A.4.5, doi: 10.1109/IRPS.2016.7574529.

[21] R. Kabouche, E. Okada, E. Dogmus, A. Linge, M. Zegaoui, and F. Medjdoub, "Power measurement setup for on-wafer large signal characterization up to Q-Band," *IEEE Microw. Compon. Lett.*, vol. 27, no. 4, pp. 419–421, Apr. 2017, doi: 10.1109/LMWC.2017.2678424.

[22] S. Demirtas and J. A. Del Alamo, "Effect of trapping on the critical voltage for degradation in GaN high electron mobility transistors," in *Proc. IEEE Int. Rel. Phys. Symp.*, Anaheim, CA, USA, 2010, pp. 134–138, doi: 10.1109/IRPS.2010.5488838.

[23] G. Meneghesso *et al.*, "Trapping and reliability issues in GaN-based MIS HEMTs with partially recessed gate," *Microelectron. Rel.*, vol. 58, pp. 151–157, Mar. 2016, doi: 10.1016/j.microrel.2015.11.024.

[24] G. Meneghesso, M. Meneghini, and E. Zanoni, "Reliability and instabilities in GaN-based HEMTs," in *Proc. IEEE Int. Conf. Electron Devices Solid-State Circuits (EDSSC)*, Chengdu, China, 2014, pp. 1–2, doi: 10.1109/EDSSC.2014.7061275.